Astron. Astrophys. 325, 255–268 (1997)

ASTRONOMY AND ASTROPHYSICS

A survey of star-forming regions in the 5 cm lines of OH⋆

A. Baudry[1], **J.F. Desmurs**[1], **T.L. Wilson**[2], **and R.J. Cohen**[3]

[1] Observatoire de l'Université de Bordeaux, URA 352 du CNRS, BP 89, F-33270 Floirac, France
[2] Max-Planck-Institut für Radioastronomie, Auf dem Hügel 69, D-53121 Bonn, Germany
[3] Nuffield Radio Astronomy Laboratories, Jodrell Bank, Macclesfield, Cheshire, SK11 9DL, UK

Received 26 September 1996 / Accepted 26 November 1996

Abstract. We have undertaken a comprehensive search for 5 cm OH masers in regions visible from Effelsberg with the 100-m telescope (i.e., those with declinations above $-29°$). Our sample is based on bright sources taken from the IRAS Point Source Catalog and/or from previous 18 cm OH and H_2O surveys. Among the 165 sources observed, 16 are new (15 exhibit emission and one source shows both absorption and emission). Two new absorption line sources have been tentatively detected. The general properties of the 5 cm OH sources are presented and discussed. The 6035 MHz line is more often detected than the 6031 MHz line. Nevertheless, the latter line is frequently present, a fact that is not explained by present OH excitation models. Simple calculations tend to show that there are enough FIR photons to pump the 6035 and 6031 MHz masers, and we found that the statistics of the ratio S_{radio}/S_{IR} at 18, 5 and 6 cm suggest that the maser pumping efficiency decreases with increasing OH excitation. Variability on short (months) or long (years) timescales is a common feature in many 5 cm OH sources. We also present observations of the 6 GHz satellite lines and report, besides W3(OH), on two certain and perhaps two newly detected weak sources. Some implications on the excitation of OH are briefly discussed. Clearly, there is no efficient maser mechanism for the satellite lines. We derive the percentage of circular polarization in detected 6035 and 6031 MHz emission sources and suggest the identifications of possible Zeeman patterns. We have found several features having $> 90\%$ polarization. Combining our magnetic field measurements with other published results we find that the dominant field alignment is consistent with the direction of the Galactic rotation. However, there is no convincing correlation of the field direction with the Galactic spiral pattern, and it is possible that the field direction is not preserved in the star formation process.

Key words: masers – stars: formation – interstellar medium: HII regions, magnetic fields – radio lines: ISM

Send offprint requests to: A. Baudry (Observatoire de Bordeaux)

⋆ Tables 1,2,4 and 6 are only available in electronic form at the CDS via anonymous ftp to cdsarc.u-strasbg.fr (130.79.128.5) or via http://cdsweb.u-strasbg.fr/Abstract.html

1. Introduction

Shortly after the discovery of intense 18 cm emission from the hydroxyl radical, OH, in W3(OH) some 30 years ago, emission from the first two excited-states of OH was also discovered (Zuckerman et al. 1968, Yen et al. 1969, for the $^2\Pi_{1/2}, J = 1/2$ and $^2\Pi_{3/2}, J = 5/2$ states, respectively). The $^2\Pi_{3/2}, J = 5/2$ excited-state of OH lies immediately above the ground-state, and thus provides a critical test for OH excitation models. The $^2\Pi_{3/2}, J = 5/2$ state gives rise to four hyperfine transitions, with the $F = 3 - 3$ and $2 - 2$ main lines at 6035.092 and 6030.747 MHz and the $F = 3 - 2$ and $2 - 3$ satellite lines at 6049.084 and 6016.746 MHz, respectively (Fig. 1). In addition, these transitions are sensitive to the magnetic field with a Landé factor $g_J = 0.485$. The theoretical treatment of OH excitation has progressed significantly in recent years, and includes many different levels, line overlap effects and accurate collision rates (e.g. Cesaroni and Walmsley 1991, Gray et al. 1992, Pavlakis and Kylafis 1996). These analyses show the importance of multi-line studies of OH sources to better understand the physical conditions prevailing in dense OH clouds.

Our goal in this work was to survey all known star-forming regions of the northern hemisphere with the 100-m telescope, and to include all of the major HII regions accessible from Effelsberg (Declinations north of $-29°$), with the exception of the Galactic Center. In our catalog of 5 cm OH targets, we used the 18 cm OH survey of Cohen et al. (1988) made for strong IRAS far-infrared sources, and we also used the most recent results of the H_2O maser surveys undertaken with the Medicina 32-m antenna (Palagi et al. 1993, Brand et al. 1994, Codella et al. 1994). The 18 cm OH masers studied by Cohen et al. (1988) are associated with far-infrared sources taken from the IRAS Point Source Catalogue and with flux densities greater than 1000 Jy at 60 and 100 μm. These sources are thus found in most of the 'classical' compact radio HII regions as well as in young objects with little radio continuum. H_2O maser emission is another well known signpost of stellar formation and is observed near to, or coincident, with diffuse HII regions and young ultra-compact HII regions. We used the Medicina H_2O survey to select sources with integrated H_2O flux densities greater than 90 Jy kms^{-1} and with 100 μm flux densities greater than 1000

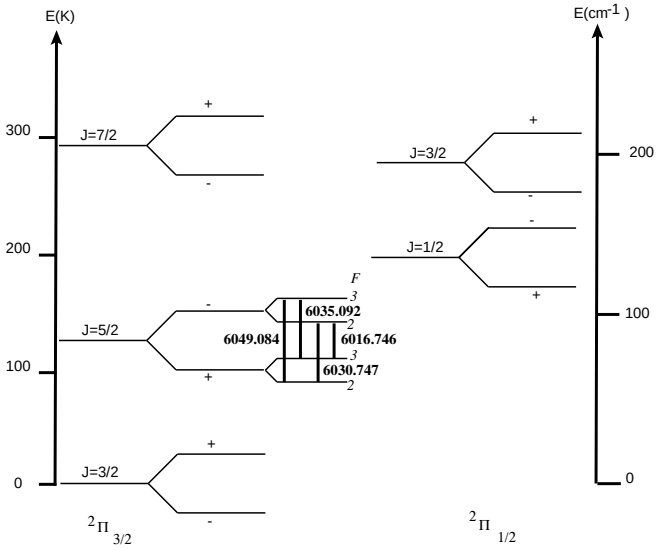

Fig. 1. The energy level diagram for the $^2\Pi_{3/2}$ and $^2\Pi_{1/2}$ ladders of the hydroxyl radical, OH. The lowest levels are shown. Transitions between the F = 3 and 2 hyperfine levels give rise to the four 6 GHz lines

Jy. We also included some other IRAS sources matching our criterion of far-infrared fluxes larger than 1000 Jy but which were not included in the Cohen et al. (1988) or in the Medicina antenna surveys. The end result was a final search list of 165 objects for 5 cm OH emission (Table 1).

We have conducted a comprehensive search with the 100-m telescope for new 5 cm OH masers. These observations, and our results are presented in Sect. 2. Of the 165 sources observed, 16 sources are newly discovered sources (15 in emission and 1 in absorption and emission). In addition, two new absorption sources have been tentatively identified, but need confirmation. Some of the emission sources were independently detected by Caswell and Vaile (1995). In Sect. 3 the general properties of the 5 cm OH sources are presented and infrared pumping and variability of main line emission sources are discussed. We also present new observations of the 6 GHz satellite lines and report, besides W3(OH), on two certain, and two possible, new detections, and discuss their implications in relation to OH excitation models. Our results for the main line OH absorption are briefly presented in the last subsection of Sect. 3. In Sect. 4 we give the percentage of circular polarization in detected sources and suggest the identifications of possible Zeeman patterns.

2. Observations and results

2.1. Observations

Observations of the main lines of OH were made with the Effelsberg 100-m telescope in the periods 1994, 12-23 May, and 1995, 22-28 July. We used a cooled HEMT dual-channel receiver to simultaneously measure right circular (RC) and left circular (LC) polarizations. The system temperature was ≈ 60 K including ground pick up and sky noise. We divided the 1024-channel autocorrelator into 4 receivers to observe both RC and LC polarizations at 6035 and 6031 MHz simultaneously. During the July observations we also separately searched for the satellite lines, simultaneously measuring both polarizations in each line. In our 1994 and 1995 observations the channel separation was 3.05 kHz, thus providing an effective resolution of 0.18 km s^{-1}. The OH spectra were calibrated in terms of the noise source coupled to both polarization channels. To calibrate the spectra we performed several azimuth and elevation scans through the planetary nebula NGC 7027. We assumed that the total flux density of NGC 7027 was 5.9 Jy at 6 GHz for our 1994 and 1995 observations (see flux density spectrum of Ott et al. 1994). With a size of 7"x10", NGC 7027 is essentially point-like in the 130" half-power beamwidth of the telescope at 6 GHz. The conversion factors are determined for both polarizations with 6 and 7 to 12% uncertainties in 1994 and 1995, respectively. Therefore, not accounting for any uncertainty in the absolute flux density of NGC 7027, we estimate that the uncertainty in our flux density scale does not exceed 10%. We calibrated all 6035 and 6031 MHz RC and LC spectra in terms of single polarization flux densities. This is one-half of the two polarization flux density. For the maser lines this procedure follows that used by Caswell and Vaile (1995).

Satellite line emission or absorption at 6049 and 6017 MHz was searched in 1995 July toward a sub-sample of 17 sources. Four of these sources as well as two other additional sources were also observed with the 100-m telescope by TLW and R. Cesaroni in 1990 August/September. The satellite line intensities and all 3 σ limits in Table 4 (satellite lines) and Table 1 (main lines) are calibrated in terms of two polarization flux densities.

All observations were made in the total power mode, and particular care was taken in looking for the possible occurrence of 5 cm radio interferences. Depending on the orientation of the antenna interferences were clearly present in a minor fraction of our data. These were easily identified as they generated a systematic ripple in the band. In this case we did not try to make any special data reduction and we simply discarded all corrupted scans.

2.2. Previous surveys and present results

Following the discovery of emission from the $^2\Pi_{3/2}, J = 5/2$ state toward W3(OH) and W75N (Yen et al. 1969, Rydbeck et al. 1970), various small scale discrete source surveys were made. Zuckerman et al. (1972) searched for the $J = 5/2$ OH in seven HII-Type I OH regions; Knowles et al. (1976) surveyed one line at 6035 MHz in more than 50 main line 18 cm OH sources of the southern hemisphere; and Guilloteau et al. (1984) surveyed 44 compact or ultra-compact HII regions. At that time the number of securely detected 5 cm OH sources amounted to 26. Recently, Caswell and Vaile (1995) searched for 6035 MHz emission in 208 OH maser sources with the Parkes 64-m telescope. The sources in their sample are south of δ = +24°, and show 1665 MHz flux densities larger than 0.8 Jy. Their survey resulted in

Table 3. Integrated flux densities of maser sources

Source	l, b	$\int$ Sdv (Jy kms^{-1})				Distance (kpc)	Luminosity (Jy kms^{-1} kpc^2)		Period[1]
		6031 MHz		6035 MHz			6031	6035	
		Right	Left	Right	Left		MHz	MHz	
W3(OH)	133.94+1.06	24.58	22.92	86.44	79.10	2.2	230	801	J
		20.68	18.24	73.22	69.62		188	691	M
05392-0214	206.83-16.49			0.04	0.05	1.8, (14.6)		0.3, (19)	M
18174-1612 (M17)	15.03-0.66			7.39	7.46	2.5		93	J
18222-1317	18.15-0.29			0.03	0.07	4.6, (11.7)		2.1, (14)	J
18274+0112 (S68)	31.58+5.34		0.03?	0.07	0.03	0.7, (13.8)		0.05, (19.0)	J
18403-0417	28.20-0.04	0.16	0.08	1.22	1.30	6.0, 8.9	8.6, 19.0	91, 200	J
		0.44	0.39	1.96	2.19		30, 66	149, 330	M
18487-0015	33.91+0.11			0.20	0.05	2.0, 12.2		1, 37	J
18507+0110	34.25+0.15			0.30	0.36	3.9, 10.16		10.0, 68	J
				0.28	0.21			7.4, 51	M
18515+0157	35.04+0.34			1.88	1.24	3.0, (10.9)		28, (371)	J
				2.03	1.60			33, (431)	M
18556+0136	35.20-0.74			0.14	0.21	2.1, 11.8		1.5, 49	J
					0.09			0.4, 13	M
18592+0108 (W48)	35.20-1.74			0.39	0.35	3.0, (10.9)		7, (88)	J
				0.97	0.58			14, (184)	M
19078+0901 (W49)	43.17+0.00			0.83	0.80	11.4		212	J
		0.20	0.20	1.10	1.10		52	286	M
19095+0930	43.79-0.12		0.04?	0.42	0.36	2.7, 9.4		5.7, 70	J
				0.54	0.56			8.0, 97	M
19111+1048	45.12+0.13	0.08	0.08?	2.48	1.72	4.1, 7.9	2.7, 10	71, 262	J
		0.08?	0.36	7.43	1.61		7.4, 27	152, 564	M
19120+1103	45.46+0.06	0.38	0.24	1.58	1.96	6.0	22	127	J
19201+1400	48.99-0.30	0.05	0.02	1.37	0.68	5.6	2.2	64	J
19213+1424 (W51 e/d)	49.49-0.37	0.36	0.50	1.85	2.13	7.0	42	195	J
19598+3324 (K3-50)	70.29+1.60	0.13	0.16	0.57	0.54	8.1	19	73	J
20081+3122	69.54-0.98	0.25	0.18	5.67	3.37	1.0, 5.0	0.4, 11	9.0, 226	J
(ON1)		0.23	0.18	3.80	2.89		0.4, 10	6.7, 167	M
20350+4126	80.87+0.42	0.13	0.16	1.33	2.29	4.8	6.7	83	J
(DR20)		0.10	0.17	1.30	*[2]		6.2	30	M
W75N	81.87+0.78			0.15	0.14	2.0		1.2	J
W75S(OH)	81.72+0.57	0.03?		0.08	0.11	2.0		.8	J
W75S(3)	81.77+0.60			0.59	0.29	2.0		3.5	J
21413+5442	98.04+1.45			0.39	0.40	7.5		44	J
				0.32	0.39			40	M
22176+6303 (S140)	106.80+5.31			0.09	0.08	1.4		0.3	J
22543+6145	109.87+2.11	0.18	0.08	0.38	0.25	0.7	0.1	0.3	J
(Cep A)		0.25	0.11	0.09	0.05		0.2	0.06	M
23116+6111	111.54+0.78			0.59	0.58	3.5		14	J
(NGC7538)				0.56	0.62			15	M

[1] J and M correspond to spectra obtained in 1995 July and 1994 May, respectively

[2] The left circular 6035MHz spectrum was strongly corrupted

the detection of 52 new 6035 MHz emission sources with peak fluxes larger than about 0.3 Jy.

Some general results of our survey in the main lines of the J = $5/2$ state are given in Table 1. We list source name, the 1950.0 coordinates, the velocity interval searched, and the 3 σ flux density limit (for no detection) or the letters E and A when an emission or absorption signal was detected. The source names given in column 2 of Table 1 are taken from the IRAS Point Source Catalog, the SIMBAD data base, or are current names. Three IRAS sources are stars, 05330−0517, 06056−0621 and 20197+3722, while IRAS 09517+6954 is the starburst galaxy M82 (note, however, that the observed velocity range is narrow −18 to 15 km s^{-1}). In general with 0.18 km s^{-1} resolution the 3 σ detection level was around 0.1 to 0.3 Jy for both the 6031 and 6035 MHz lines and for both polarizations. Among the 165 sources in Table 1, twenty-five show emission profiles, two a mixture of absorption and emission, and one, perhaps three, show absorption. Table 1 contains 12 previously known 5 cm OH sources as well as 16 new discoveries, perhaps 18 (including 2 possible absorption sources); six among these 18 were independently discovered in 6035 MHz emission by Caswell and Vaile. It is important to note that 18222−1317 exhibits both weak absorption and emission at 6035 MHz and that this source was not previously listed in catalogs of OH, H_2O or CH_3OH maser sources. IRAS 18222−1317 also exhibits CS molecular line emission (Bronfman et al. 1996) at a velocity close to our OH detection, and was mapped in the radio continuum by Kurtz et al. (1994). The spectra of the 15 new sources observed in 1995 are shown in Fig. 2. (05392 − 0214 discovered in 1994 was not detected in 1995 and seems to be variable.) The line parameters of all detected OH main line sources are given in Tables 2 and 5 for emission and absorption, respectively. Although the emission features are not necessarily gaussian, the full linewidths at half peak intensity, peak flux intensities, and associated velocities were obtained from a multi-gaussian fit analysis. (In some cases this may give peak intensities slightly different from the actual peak flux densities in our spectra.) When an emission feature is present in only one spectral channel, the linewidth is taken to be equal to the spectral resolution. Although variability is observed in several sources (see Sect. 3.1) we have not observed line shifts of a given feature exceeding our spectral resolution. In Table 2 we list all emission sources detected in 1995 July and the line parameters of those features (marked with an asterisk in the column "Line identification number") which were present in our 1994 May data only. In some sources we cannot exclude the presence of broad, weak, underlying features (i.e. features broader than 5 to 10 km s^{-1} and with intensities around 3 times the r.m.s. noise). This is probably the case for 18403−0417 where broad emission wings seem overwhelmed by strong narrow emission lines in our 6035 MHz spectrum. No attempts were made to fit broad *emission* features in our data as such features are rare in excited-states of OH and difficult to identify. (See, however, analysis of the satellite line emission from W3(OH) in Sect. 3.2.) In order to estimate variability in our 5 cm OH sources we gather the integrated flux densities of our 1994 and 1995 observations in Table 3. We also give in Table 3 the galactic coordinates and the apparent maser luminosity (in Jy km s^{-1} kpc^2) defined here as the sum of the RC and LC integrated flux densities times the distance squared. This apparent luminosity is transformed into isotropic luminosity once the distance is known after multiplication by 6.3 10^{-9} $L_\odot$ Jy^{-1} km^{-1} s kpc^{-2}. The source distance is based either on spectrophotometric estimates or, more often, on our own kinematical distance calculation program using the standard IAU galactic rotation constants; in the case of distance ambiguity the less plausible solution is given in parentheses. In W3(OH) the 6035 MHz isotropic luminosity is $\approx 4 - 5\ 10^{-6}$ $L_\odot$.

Table 5. Line parameters of absorption sources

Source	Line	LSR Velocity (kms^{-1})	Linewidth (kms^{-1})	Peak flux density (Jy)
02219+6152 (W3A)	6035	-39.71	2.86	-0.38
	6031	-39.45	3.49	-0.41
18222-1317 [3] (RAFGL 2147)	6035	+58.37	(0.30)	-0.40
18592+0108 [3] (W48)	6035	42.44	2.54	-0.19
	6031	42.44	2.54	-0.19

[3] See text for derivation of line parameters

A sub-sample of 17 sources in Table 1 and two other sources (G10.6−0.4 and K3 − 50) were searched for satellite line emission. The results of this search are presented in Table 4 which comprises most of the strongest main line emission sources, one absorption source W3A, and 4 sources with no detected emission or absorption main line signal. After data editing and averaging left and right circular polarizations the 3 σ limit in our final spectra ranges from 60 to 150 mJy for both satellite lines. However, in 5 sources W3A, W3(OH), G10.6 − 0.4, K3 − 50 and NGC 7538 the integration time was longer than the typical 30 to 50 minutes used for other sources in Table 4; this resulted in a 3 σ limit around 40−60 mJy or better. Weak satellite lines were detected in W3A, W3(OH), G10.6−0.4 and very likely in K3 − 50 and NGC 7538 (IRS2) but no intense maser emission was observed.

3. General properties and excitation of 5 cm OH sources

3.1. Main line emission sources

3.1.1. Line intensity, linewidth, and velocity extent

The peak flux densities observed in this work range from about 115 Jy in W3(OH) at 6035 MHz to about 0.1 Jy in S 68 or Cepheus A at 6031 MHz. Emission from the northern hemisphere source W3(OH) is exceptionally strong and is comparable to the 140 Jy emission reported by Caswell and Vaile for 351.42+0.64 in the southern hemisphere. M17 (18174−1612), ON1 and 20350 +4126 with peak flux densities around 12−14

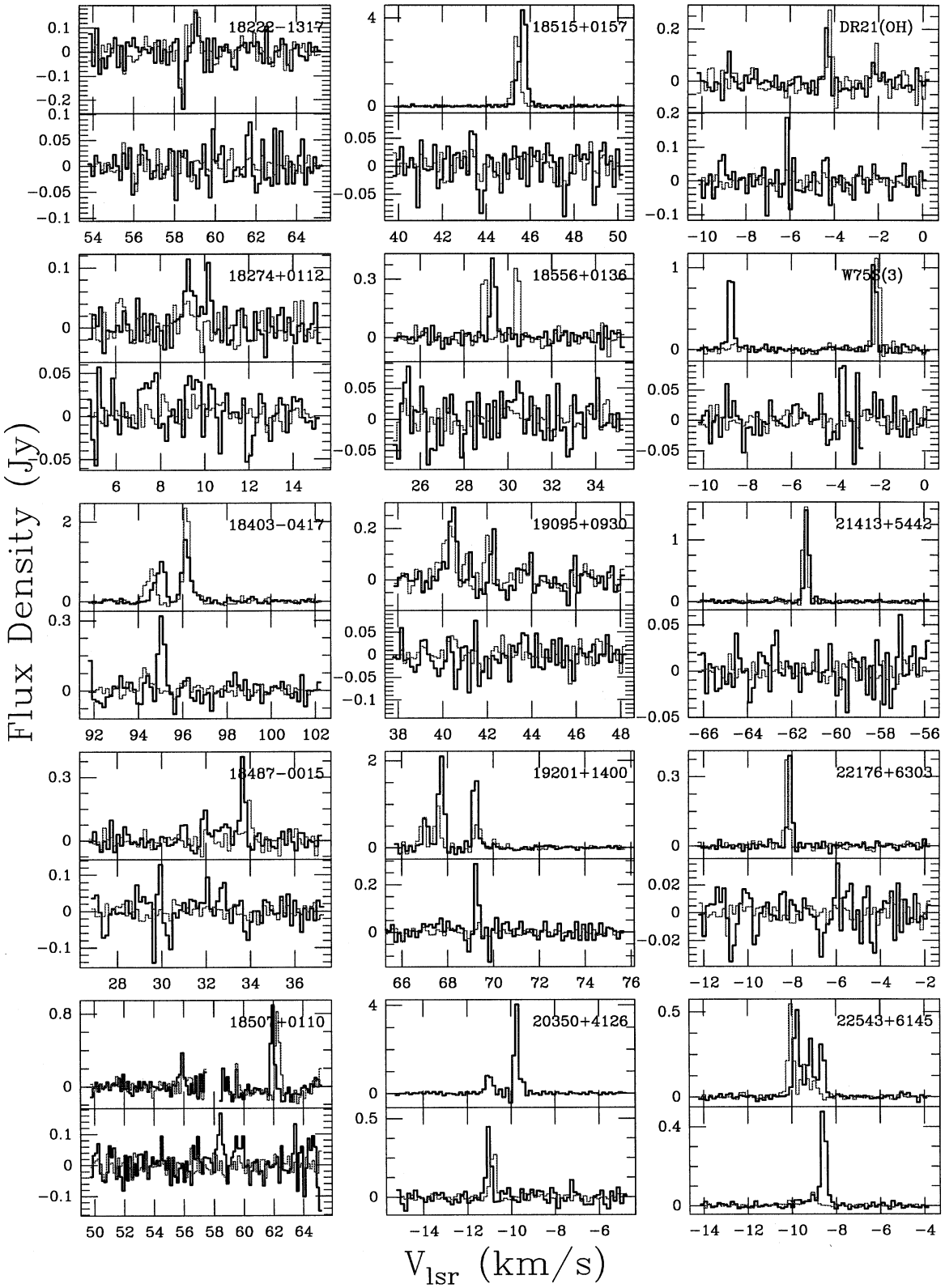

Fig. 2. The 6 GHz spectra (6.035 GHz, $F = 3 - 3$ above and 6.031 GHz, $F = 2 - 2$ below) obtained in 1995 for those sources discovered in our survey. The line intensities are in Jy for a single polarization. The thicker lines are right circular (RC) polarization, the thinner are left circular (LC)

Jy at 6035 MHz are three other relatively strong OH sources in our sample. Nevertheless, the 5 cm OH emission is weak compared to the ground-state emission and, apart from three sources in our list, the flux densities are much greater at 1665 than at 6035 MHz (see also end of Sect. 3.1.2). W3(OH) is an intermediate case with 6035 MHz flux densities comparable with those at 1665 MHz.

Prior to our observations, the properties of the F = 2 − 2 line at 6031 MHz were poorly known because this line was often not observed. The 6031 MHz emission is always weaker than the 6035 MHz emission as shown in Tables 2 and 3, and with the exception of ON1 and W3(OH) the peak flux densities are below 0.5 to 0.8 Jy . In sources where both the $F = 3 - 3$ and $2 - 2$ lines are detected, the $F = 3 - 3/F = 2 - 2$ peak flux ratio varies from 2 to 7 (e.g. W49 or ON1) to even larger values (19111+1048). In the exceptional case of Cep A this ratio is of order unity. Similarly, the $F = 3 - 3/F = 2 - 2$ integrated flux density ratios range from 1 or 2 to 20 or 30. In the LTE approximation the $F = 3 - 3/F = 2 - 2$ ratio is $20/14 \approx 1.4$ in the optically thin case, and tends towards unity in the optically thick case. Therefore, non-LTE ratios are observed in all sources. This property, together with strong polarization of the emission lines (see Section 5) and narrow linewidths (see below) are strong indications that the 6035 and 6031 MHz line emission is caused by the maser process. A definitive proof of the maser nature of the 5 cm emission is given by VLBI observations of HII regions (Moran et al. 1978, Desmurs et al. 1996).

Table 2 contains 161 and 57 circularly polarized features at 6035 and 6031 MHz, respectively. The richest spectra are those of W3(OH), W49, 19120+1103, 19213+1424 (W 51), and ON1 with 10 to 20 individual features at 6035 MHz. These sources also exhibit 6031 MHz emission. The distribution of linewidths (Fig. 3) shows that: (i) The 6035 and 6031 MHz linewidths are similar, $(ii) \approx 65\%$ of the 6035 MHz features are narrower than 0.35 km s^{-1}, and (iii) Several 6035 and some 6031 MHz sources have features as sharp as 0.18 km s^{-1} our spectral resolution. This suggests that the intrinsic linewidth of several features might be narrower than 0.18 km s^{-1}. There is no apparent correlation of linewidth with peak intensity in our data. In W3(OH), the strongest source in the northern sky, peak fluxes of identified features range over more than 2 orders of magnitude and their linewidths remain remarkably constant, being around 0.3 to 0.4 km s^{-1}. As indicated above several sources exhibit features $\leq$ 0.18 km s^{-1}. This cannot directly reflect the kinetic temperature of the gas, since a Doppler width $\leq$ 0.18 km s^{-1} would correspond to about 10 K or less whereas we expect $T_K \approx 150$ K in the vicinity of compact HII regions (see the multi-line OH analysis of Wilson et al. 1990). In the strict case of non-saturated masers the line narrowing scales with $\tau^{-1/2}$, where τ is the opacity at the line center; we would thus expect $\tau \geq 12$ for $T_K \approx 150$ K.

The 5 cm OH velocity extent typically ranges from 1 km s^{-1} in Cep A or W 48 to 7 km s^{-1} in W75(OH) or W3(OH), whereas the 18 cm OH velocity extent is roughly 10 km s^{-1}. W 49 and ON1 appear to be quite exceptional. W49 emission

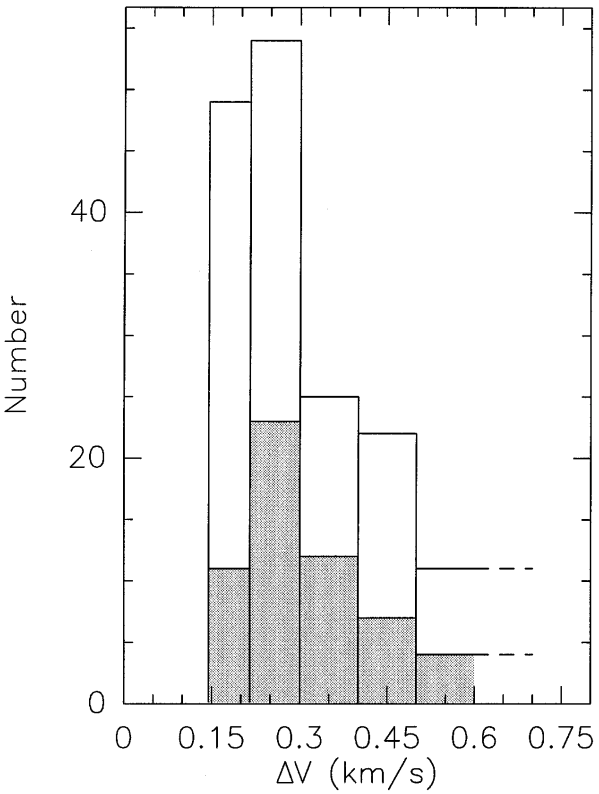

Fig. 3. Histograms of the FWHP linewidths for the $F = 3 - 3$, 6.035 GHz and $F = 2 - 2$, 6.031 GHz (shaded histogram) OH lines measured in this survey. For those lines narrower than our effective resolution, 0.18 km s^{-1}, we have used a linewidth of 0.18 km s^{-1}

extends at least over 10 km s^{-1}, and in ON1 we observed two groups of features separated by about 15 km s^{-1}. The detection with high signal to noise ratio of strongly polarized 6035 MHz OH emission around -1 to 1.5 km s^{-1} toward ON1 (Fig. 4) had not been reported previously as far as we are aware, although 18 cm OH features at 2 and -6 km s^{-1} were observed by Cohen and Willson (1981). This 6035 MHz emission was clearly detected in both 1994 and 1995 data. Note that the ratio of the peak intensity around 14 km s^{-1} to the peak intensity around -1 to 1.5 km s^{-1} remains roughly constant with time (see Fig. 4 and note that at 6035 MHz the intensity scale around 14 and 0 km s^{-1} are different). However, both groups of 6035 MHz lines vary with time and such variation cannot be caused by pointing or calibration errors since the simultaneously measured 6031 MHz line data remain constant. We conclude that the lines around 0 and 14 km s^{-1} arise from the same region.

The OH maser model developed by Cesaroni and Walmsley (1991) which includes effects of local and non-local line overlaps and the IR radiation from hot dust, predicts an inversion of the 6035 MHz line for H_2 densities $\approx 10^6$ to a few 10^7 cm^{-3} and no inversion at 6031 MHz. This is roughly consistent with our observations which show that the 6035 MHz line is more intense and more widely detected than the 6031 MHz line. Nevertheless, the present work and recent 6031 MHz VLBI observations of W3(OH) (Desmurs et al. 1996) demonstrate that the 6031

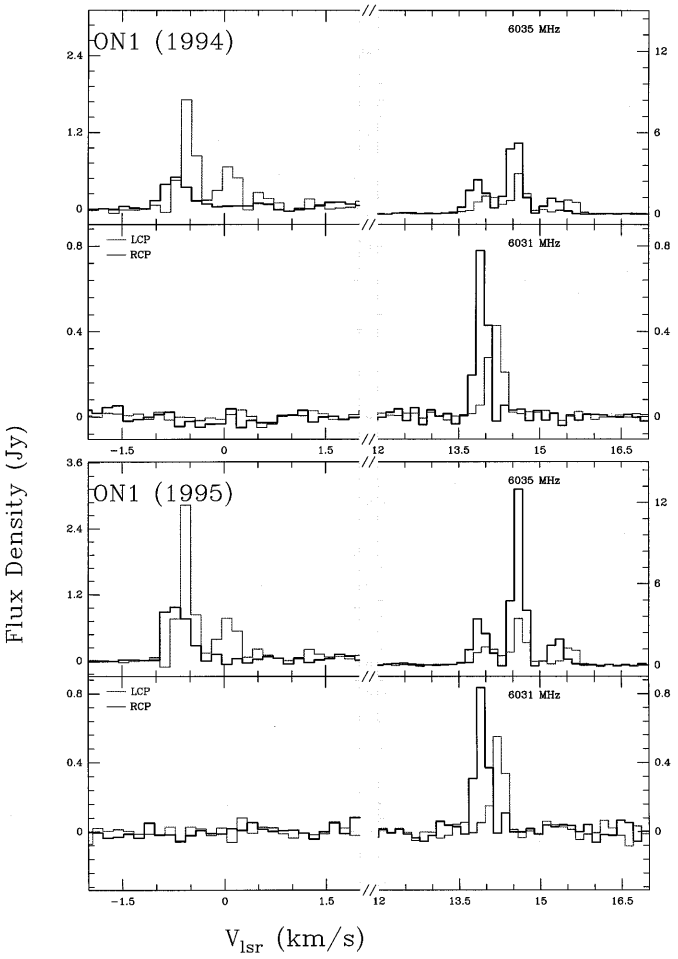

Fig. 4. Spectra of the 6.035 GHz (upper) and 6.031 GHz (lower) OH lines measured in May 1994 for the source ON1, in the upper panel. In the lower panel, these lines are measured in July 1995. The thicker lines are right circular polarization, the thinner are left circular. Note that at 6.035 GHz the flux density scales are different for features around 0 and 14 km s^{-1}

MHz line is masing whereas the Cesaroni and Walmsley model does not predict inversion of this line and faces other difficulties (see end of Sect. 3.2). The OH model of Gray et al. (1991, 1992) predicts the inversion of both 6035 and 6031 MHz lines with stronger emission at 6035 MHz for H_2 densities greater than a few 10^7 cm^{-3}, but this requires (i) the absence of overlap, which is a key feature of all ground-state OH maser excitation models, and (ii) high OH relative abundances ($OH/H_2 \approx 10^{-5}$) to yield bright 6035 MHz emission. One major difficulty faced by OH excitation models is their dependence on exact collision rate coefficients as shown by Pavlakis and Kylafis (1996). For this reason and in the absence of all needed coefficients, Pavlakis and Kylafis did not discuss their results for the $^2\Pi_{3/2}$, $J = 5/2$ masers and restricted their analysis to the 18 and 6 cm lines. In conclusion, it is impossible to deduce precise physical conditions from a comparison of 6 GHz observations with OH models. However, all models require H_2 densities of order 10^7 cm^{-3}.

3.1.2. Infrared pumping

Excitation of the OH radical results from complex competitive schemes involving both collisional and radiative pumping as well as line overlap effects in relation with the velocity field in the OH medium and local line broadening. In order to evaluate in very simple terms the role played by IR photons in the 5 cm OH masers we note that, with no absorption of far infrared photons, radiative pumping is possible when

$$(\int S d\nu Sh\nu)_{IR}\, \Omega_{IR} \geq (\int S d\nu Sh\nu)_{radio}\, \Omega_{radio}$$

where Ω_{radio} is the maser beam angle and Ω_{IR} is the solid angle subtended by the maser at the IR source. Assuming that all masers associated with each source spectrum are pumped by IR radiation and that the mean beam angle ratio for each source is $< \Omega_{radio}/\Omega_{IR} > \approx 1$ we must now verify that

$$S_{IR} \Delta v_{IR} \geq (\int S dv)_{radio}$$

where S_{IR} is the IR peak flux, Δv_{IR} the range of radial velocity across the OH maser spectrum, and $(\int S dv)_{radio}$ the integrated maser flux density. The 5 cm OH lines arise from energy levels 84 cm^{-1} above the ground-state and we expect that FIR photons around 100 μm are involved in the OH pumping cycle. In Fig. 5 we have plotted the 6035 MHz OH integrated flux density measured in this work, adding both polarizations, versus the IRAS 60 μm flux density times Δv_{IR} determined from the total OH spectral extent of each observed source. The condition above is also held at 100 μm, and is even better held at 6031 MHz where the radio flux densities are weaker than at 6035 MHz. Despite the uncertainties of this simple approach, we note that there are more FIR photons than radio photons by roughly four orders of magnitude. Therefore, even if the IRAS field of view picked up more FIR flux than that directly coming from the compact HII region it seems that there are enough FIR photons to pump the 6035/6031 MHz OH masers. In a similar study made for 18 cm OH sources, Moore et al. (1988) showed that there is a correlation between the OH 1665 MHz peak flux density and the FIR flux density, and concluded that 18 cm OH masers are pumped by FIR photons. These photons clearly play a dominant role in the $^2\Pi_{3/2}$ ladder since the correct parity assignment in the collision rates (Andresen et al. 1984) showed that collisions alone cannot invert the OH lambda-doublets in the $^2\Pi_{3/2}$ ladder. Of course the OH net inversion depends on detailed balance between radiation pumping and collisional deexcitation (e.g. Cesaroni and Walmsley 1991). Moreover, it is interesting to note that in order to produce maser inversion one must fulfill the thermodynamic constraint where more than one IR photon must escape the inverted region for every maser photon. In the case of 100 μm photons escaping 6 GHz masing cylinders and assuming a gas kinetic temperature around 150 K, equation (3) of Watson (1993) yields for the maser brightness temperature $T_m < 2.5\ 10^8 (l/d)^3$ where l/d is the cylinder aspect ratio. For $T_m \approx 1.4\ 10^9 - 10^{10}$ K corresponding to $1-10$ Jy features with typical sizes ≈ 5 mas (Desmurs et al. 1996) we expect typical aspect ratios larger than 3.

The ratio S_{radio}/S_{IR} was also considered by Cohen et al. (1991) in their study of OH 6 cm maser sources in IRAS-selected star-forming regions. They found that the median value of this

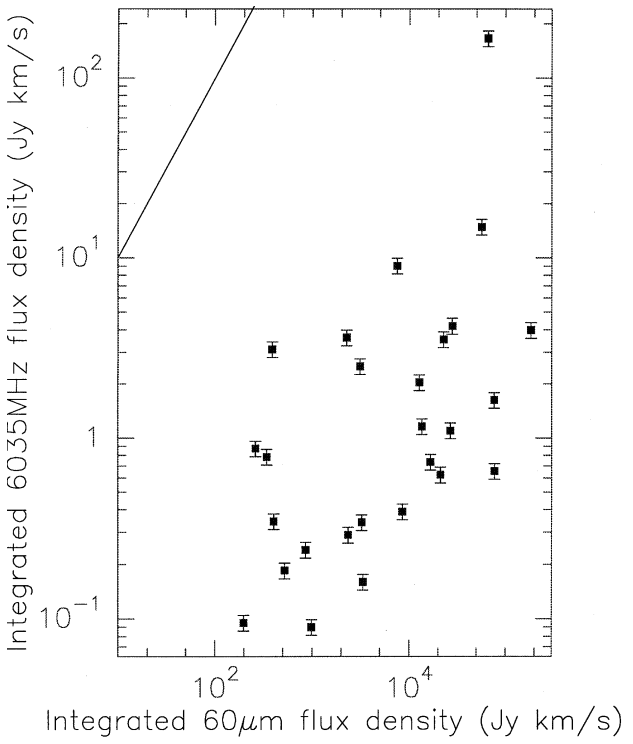

Fig. 5. A plot of the flux density of the 6.035 GHz line, integrated over velocity, versus the 60 μm IRAS flux density, multiplied by the total 6 GHz OH velocity range. The smooth line shows the locus of points where the OH and IR integrated fluxes are equal

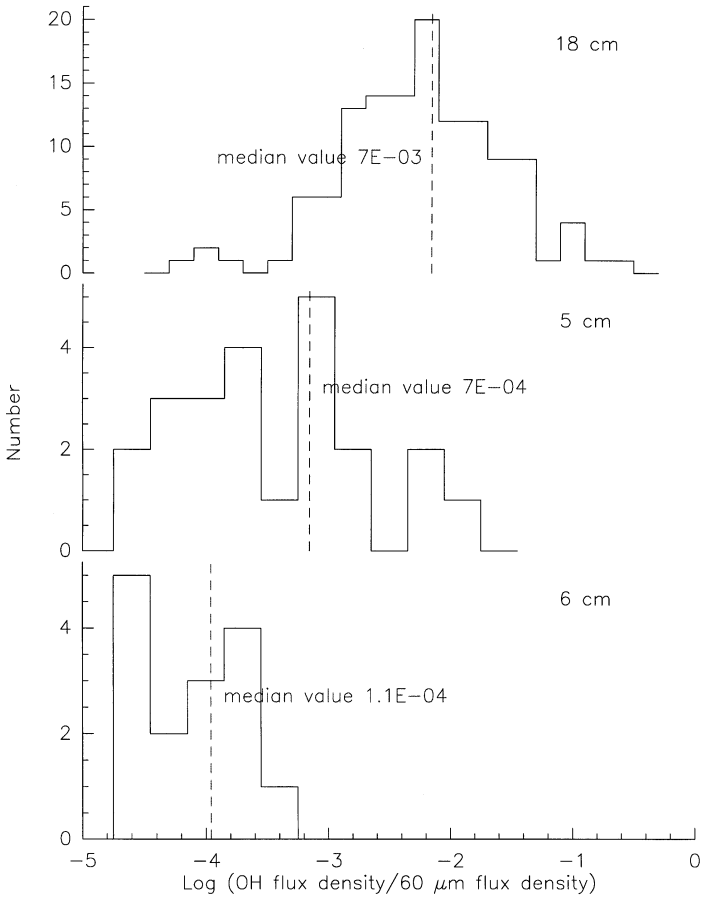

Fig. 6. For the sources detected in this survey, we show three histograms of the ratios of OH to 60μm IR flux densities for 18 cm (Cohen et al. 1995), 6 cm (Moore et al. 1988) and 5 cm (this paper)

ratio was two orders of magnitude lower for OH 6 cm masers than for OH 18 cm masers. In Fig. 6 we compare results at 6 cm taken from Cohen et al. (1991) and from more recent work by Cohen et al. (1995) with those from the present work on OH 5 cm masers and those from Moore et al. (1988) on OH 18 cm masers. The 5 and 18 cm lines are polarized, so we have added the LC and RC intensities to derive the peak flux densities. We have used only the IRAS fluxes at 60 μm since the 60 and 100 μm correlations with OH integrated intensities are very similar. Fig. 6 shows a systematic decrease in the ratio S_{radio}/S_{IR} with increasing OH excitation. The median value is 7 10^{-3} for 18 cm OH, 7 10^{-4} for 5 cm OH, and 1.1 10^{-4} for 6 cm OH. This suggests that the maser pumping efficiency decreases systematically with increasing energy above the ground-state. In fact such a result was nicely demonstrated for the source W3(OH) by Cesaroni and Walmsley (1991), whose figure 11 shows maser optical depth falling systematically with increasing excitation energy. However, this is the first time that data have been available for a large number of sources to allow the general statistics of the radio-IR correlation to be examined in several OH lines. The data of Fig. 6 should provide important input to a new generation of more accurate maser models which treat simultaneously and self-consistently the OH excitation and radiative transfer. In addition, we note that when comparing the 6035 and 1665 flux densities, only 3 out of the 26 sources in our list (namely M17, OH45.12+0.3 and ON1) exhibit intensities *greater* at 6035 than at 1665 MHz. Therefore, assuming that time variability is a small effect this seems to be a rare occurrence, M17 being an extreme case with S(6035) $\approx$ 4.7 S(1665).

3.1.3. Variability

Table 3 shows that fourteen sources were observed twice, and that variability is present in several sources. In the time interval between our 1994 May and 1995 July observations the 6035 MHz integrated intensities (LC + RC) vary from about 15 % (W3(OH)) to 55 % (e.g. W48 or 19111+1048). Variability is even more prominent in 18556+0136 and Cep A for which the 6035 MHz flux density increased by a factor of 3−3.5 from 1994 to 1995. Since the total uncertainty due to instrumental factors for both epochs amounts to about 10 − 12% (see Sect. 2.1), variability is well established. In W3(OH), however, we cannot firmly conclude on variability. We point out that eventual telescope pointing errors do not play a role in the observed variability because the individual (VLBI) hot spots associated with 6035 MHz line features are distributed over compact regions (less than 0.5 arc sec, Desmurs et al. 1996) which are thus much smaller than the 100-m beamwidth. We also note that when the 6031 MHz line is detected at both epochs, the

integrated intensity tends to vary in the same sense as that of the 6035 MHz line suggesting that both lines are excited in the same gas layers and/or that the same pumping mechanisms are at work for both lines. There is one exception, however, that of Cep A whose time variability in the 6035/6031 intensity ratio should be carefully monitored.

Several sources were observed at 6035 MHz over a 6-month time scale by Caswell and Vaile. Some changes were observed but most sources do not exhibit changes greater than 10 %. It is interesting to note that Rydbeck et al. (1970) observed strong time variability within two months in W75B. These results, and our observations over a 14-month interval indicate that variability exists over several characteristic time intervals. We find indications of variability over an even shorter time scale since eight sources in our sample, 18403−0417, 18507+0110, 18515+0157, 18556+0136, 18592+0108 (W 48), 19078+0901 (W 49), 19095+0930, and 19111+1048 were observed on 1994 May 20 and by Caswell and Vaile on March 21−25. The line profiles, sense of polarization, and peak intensities obtained with both Parkes and Effelsberg telescopes are similar for most sources, despite the fact that the source coordinates are not always identical. However, for W48 and W49, the relative intensity of some 6035 MHz features and the peak fluxes changed markedly with time. These changes indicate rapid time variations at 6035 MHz, thus implying typical maser sizes smaller than c $\Delta t \approx 1.5\ 10^{17}$ cm ≈ 0.05 pc for $\Delta t = 58$ days.

Several intense OH sources have now been studied over more than 20 years. It is remarkable that the spectral profile of W3(OH) has remained stable over 25 years. This suggests to us that saturated maser amplification takes place in strong sources. M17, the strongest source in our sample after W3(OH), was observed by us in 1995 July, by Caswell and Vaile in 1993 and 1994, and by Knowles et al. (1976). The 6035 MHz spectrum has remained essentially unchanged with two main features around 21.5 and 22.6 km s^{-1} but with differing relative intensities. ON1, another strong 5 cm OH source was observed in circular polarization by Rickard et al. (1975). Comparing their intensity scale with ours is complicated. However, we find that their three main features, around 14.5 km s^{-1}, are present in our spectra (but with some differences in relative intensity). These comparisons suggest that the strongest sources are saturated masers. Nevertheless, long term variability is present in the 5 cm OH spectra, since both relative and absolute intensities of individual features do change with time. In addition, for several sources studied at Parkes over a time interval of 20 years, Caswell and Vaile have noted large intensity changes in many features. This seems to be the case of Orion A for which the flux density is now below 0.3 Jy (see our Table 1), but which was around 2 Jy in each circular polarization at the time of the discovery by Knowles et al. (1976).

3.2. Satellite line sources

Satellite line emission or absorption was searched toward 19 sources (Table 4). The 3 σ limits achieved in our final spectra (see Sect. 2.2) are better or much better than those achieved for the main lines. However, we do not reach the LTE intensity limit, in which the 6017 and 6049 MHz lines are respectively 14 and 20 times weaker than the sum of the RC and LC main lines. From Table 4 we conclude that 5 cm satellite line radiation is very weak and that strong satellite line masers are not excited in the $J = 5/2$ state of OH, although more observations undertaken at different epochs should be repeated to reach firmer conclusions. Even in the strongest OH source in the northern sky, W3(OH), for which we have now several epoch satellite line observations (see below), there is no trace of intense maser activity.

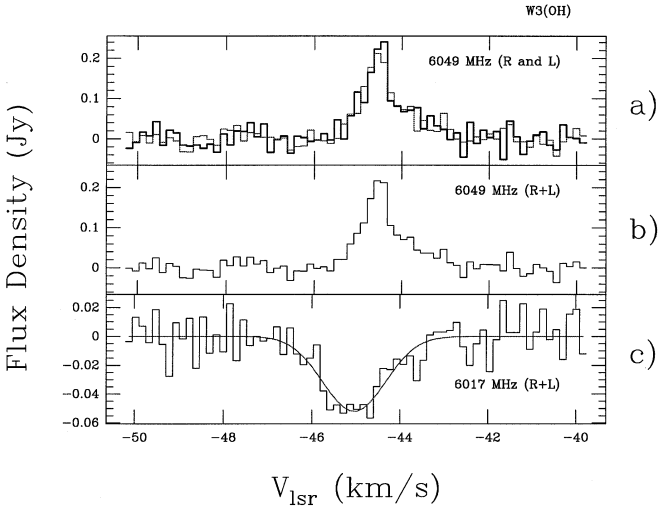

Fig. 7a–c. The 6 GHz OH satellite lines. In **a** the ($F = 3 - 2$) 6.049 GHz line (RC heavy, LC light contours). In **b** the sum of RC and LC for the 6.049 GHz line, and in **c** the 6.017 GHz ($F = 2 - 3$) OH line. The intensity scales in **a** is the single polarization flux density, in Jy. In **b** and **c** this is the flux density for both polarizations. The continuous line in **c** corresponds to the gaussian fit discussed in Sect. 3.2

W3(OH) was observed in the satellite lines with the 100-m radiotelescope in 1981 (Guilloteau et al. 1984), 1989 (Kempf 1989), 1990 August, and 1995 July. Fig. 7a–c shows our best spectra obtained in 1995 after more than 2 hours of integration in each sense of polarization. Line parameters of the 6017 and 6049 MHz transitions are very similar in both polarizations; this is shown for example at 6049 MHz in Fig.7a–ca. Panels b and c show the average of RC and LC 6049 and 6017 MHz spectra. The gaussian fit parameters to the averaged spectra are the following: $S_{peak} = -54$ mJy (1 σ = 14 mJy), $\Delta v = 1.89 \pm 0.27$, $V_{LSR} = -45.02 \pm 0.10$ for the 6017 MHz line; $S_{peak} = +180$ mJy (1 σ = 14 mJy), $\Delta v = 0.86 \pm 0.07$, $V_{LSR} = -44.54 \pm 0.02$ for the 6049 MHz line. In the latter case the slightly asymmetric line profile could also be fitted by 2 nearby Gaussians with 155 and 60 mJy peak fluxes, and 0.51 and 1.67 km s^{-1} linewidths, respectively. Guilloteau et al. (1984) detected satellite line emission at 6049 MHz with peak intensity and central velocity similar to ours but with a broader linewidth. They failed to detect the very faint 6017 MHz line absorption. Subsequent observations made in 1989 and 1990 compared with our 1995 data show that the satellite line profiles are essentially stable with time.

Taking $S_{cont} \approx 0.7$ Jy at 6 GHz we find that the apparent peak opacities are of the order of -0.2 and 0.08 for the emission and absorption, respectively. The actual opacities must be higher since VLA data show that the OH material does not cover the entire continuum source (e.g. Baudry and Menten 1995). The 6049 MHz emission line could correspond to a low gain maser. Such cases have been observed in the transitions from the $^2\Pi_{1/2}$ ladder (Baudry et al. 1993). We also note that the satellite absorption and emission line centers, although falling within the OH velocity range do not coincide with the strongest 6035/6031 MHz maser features; rather these seem to be associated with the absorption features observed in several other excited-OH states and in particular with the $^2\Pi_{1/2}$ absorption lines detected by Wilson et al. (1990) and mapped by Baudry et al. (1993). We conclude that there is no indication of strong maser activity in the 6 GHz satellite lines because: (i) The line profiles are strikingly similar in both polarizations; (ii) The emission line is weak with a peak flux of ≈ 0.18 Jy and a linewidth larger than the average 5 cm maser linewidth; and (iii) There is no indication of variability in our spectra spanning the interval 1981-1995.

In addition to the W3(OH) results, our long integration observations of 1990 show that weak emission or absorption is detectable in some sources. We briefly discuss these results. Toward W3, at a position slightly different from W3A in Table 1 (RA = $2^h21^m50.4^s$ (1950) Dec= +61°52'17"), our 1990 spectra show a broad 6017 MHz absorption. This absorption is centered at ≈ -40 km s^{-1} with a linewidth and peak flux around 2.5 km s^{-1} and 60 mJy (1 $\sigma \approx 20$ mJy). This peak flux density is consistent with the 3 σ limit in our 1995 spectra, and the linewidth and center velocity are also consistent with our 6031/6035 MHz observations of 1995 (see Table 5). In W3A we can apply the sum rule to the apparent opacities or flux densities, writing $S(6031)/14+S(6035)/20 = S(6017)+S(6049)$. Taking the flux densities measured at 6031, 6035 and 6017 MHz we obtain $S(6031)/14+S(6035)/20 \approx 50$ mJy which is consistent, to within the uncertainties, with the non-detection of the 6049 MHz line. W3 (continuum) was also observed by Gardner and Martín-Pintado (1983b) who detected weak 6017 MHz absorption consistent with our results. G10.6 $-$ 0.4 is an ultra-compact HII region (RA = $18^h07^m30.7^s$ (1950) Dec=$-$19°56'31") which we observed in both satellite lines. A weak 6017 MHz absorption was detected at ≈ -3 km s^{-1} on two different days. The linewidth and peak flux density are of order 4.5 km s^{-1} and 35 mJy (1 $\sigma \approx 15$ mJy), respectively. At 6049 MHz, a 45 mJy (1 $\sigma \approx 15$ mJy) and 4.5 to 5 km s^{-1} wide emission was detected at ≈ -2 km s^{-1}. This result is in good agreement with the J = 1/2, 6 cm line OH parameters determined by Gardner and Martín-Pintado (1983a) and Guilloteau et al. (1988). It is interesting to note that the 6035 MHz observations of this source by Caswell and Vaile revealed only weak (≈ 0.2 Jy) emission. Although the continuum emission from G10.6 $-$ 0.4 resembles that of W3(OH), the OH excitation properties of these sources are quite different. K3 $-$ 50 and NGC 7538 are two other ultra-compact HII regions similar to W3(OH) and G10.6 $-$ 0.4; these were observed at positions given in Table 1. Weak (40 to 20 mJy) 6049 MHz emission was detected in K3 $-$ 50 and NGC 7538 at ≈ -20 and -59 km s^{-1}, respectively. The linewidths are uncertain, and this is why "?" is added after the letter E in Table 4. Finally, we note that in two other sources which were not observed here in the satellite lines, W33 and DR21, weak satellite lines were detected by Gardner and Martín-Pintado (1983b).

The 6 GHz satellite lines are not easily explained and strongly constrain any future OH models. The model of Cesaroni and Walmsley (1991) predicts no inversion at 6017 MHz whereas the 6049 MHz line should be strongly inverted. This is in contradiction with our observations of weak 6049 MHz emission in W3(OH) and three other sources, although the 6017 MHz line is not inverted in our spectra. With or without line overlap, Gray et al. (1991) predict both 6049 and 6017 MHz inversions. However, *no* emission has *ever* been observed from the 6017 MHz line. Finally, it is important to note that no reliable prediction of the excitation of the 5 cm lines can be made with insufficient knowledge of collision rates (see Pavlakis and Kylafis 1996, and the end of Sect. 3.1.1).

3.3. Main line absorption sources

OH absorption features were definitely detected in three and, perhaps in five sources of our sample (Table 1). Except in the case of W3A where we used 0.6 km s^{-1} resolution, the spectral resolution was 0.18 km s^{-1} everywhere. The line parameters of the definite detections of OH $^2\Pi_{3/2}$, J = 5/2 absorption are given in Table 5. Two sources exhibit both absorption and emission (18222$-$1317 and W 48). In two other sources, RAFGL 5456 and RAFGL 2210 (18355$-$0650), we observed possible absorptions around 27 and 43 km s^{-1}. However, because of the shortness of the integration time these detections are tentative, and require confirmation.

For W3A the line parameters were obtained from our 1994 spectra after we had averaged LC and RC spectra and after we had verified that each circularly polarized profile gave consistent results. The peak flux densities of both main lines are similar. This fact and the rather large widths of the absorptions, of order 2.5$-$3.5 km s^{-1} compared to less than 0.35 km s^{-1} for maser features in general, suggest a quasi-thermal excitation of these lines. In such a case we expect 6035/6031 intensity ratios in the range 20/14 to 1 for the optically thin and thick cases. This is in approximate agreement with the observations. RAFGL 2147, or 18222$-$1317, a new OH source (cf. brief discusssion in Sect. 2.2), is a different case because both absorption and emission are present. Our best fits to the spectra are given in Tables 2 and 5 for the emission and absorption, respectively. These line parameters are uncertain because the signal-to-noise ratios are low and the emission seems to be located on the edge of the absorption profile. Therefore the linewidth of 0.3 km s^{-1}($FWHP$) quoted for the absorption must be considered a lower limit. In W48, or18592+0108, both weak absorption and strong emission are present in the 6035 MHz profile. We first used high quality 6031 MHz RC and LC polarized spectra to determine line parameters for an average from our 1994 and 1995 observations. We then made a Gaussian fit of the 6035 MHz absorption intensity and of all line parameters of the two

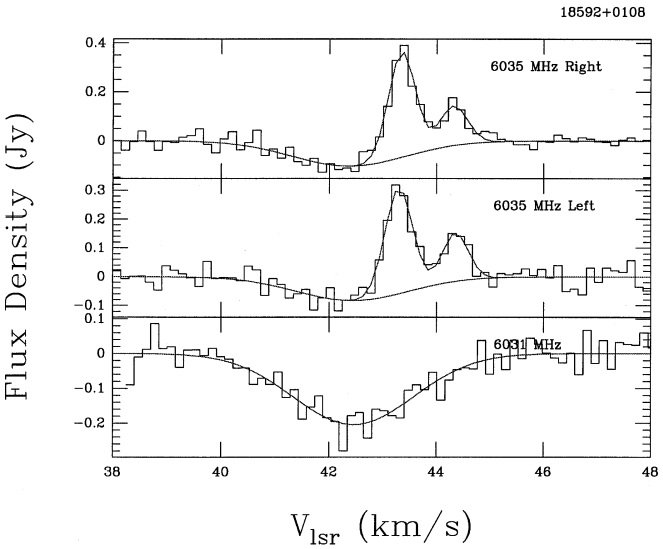

Fig. 8. In the upper two panels, the RC and LC polarized spectra for 6.035 GHz in W48 observed in July 1995. The intensities are for a single polarization. In the bottom panel is the 6.031 GHz spectrum with double polarization flux density scale. In this case the profile is an average from our 1994 and 1995 observations (see text)

emission features after we had fixed the linewidth and center velocity of the absorption feature, under the assumption that these parameters are similar to those in our averaged 6031 MHz LC + RC profile. The line parameters of the emission features are given in Table 2. The 6035 MHz absorption intensity from the averaged RC and LC profile is -0.19 Jy, a value exactly equal to the 6031 MHz absorption intensity (Table 5). The 6031 and 6035 MHz profiles of W48 are presented in Fig. 8.

4. Circular polarization and Zeeman splitting of OH main lines

Our 6031/6035 MHz profiles are often circularly polarized, and this polarization is best expressed as $P = (V/I)$ where I is the total intensity and V the difference between the right circularly and left circularly polarized intensities. Although a complete description of polarized radiation would require a measurement of all Stokes parameters, the percentage of circular polarization is directly given by the two Stokes parameters V and I and by the quantity P defined above. Our observations are not sensitive to linear polarization, and we assume that this can be neglected because no or little linear polarization was detected in the $J = 5/2$ OH sources observed by Zuckerman et al. (1972) and Rickard et al. (1975). Therefore, by deriving the ratio $|S_R - S_L|/(S_R + S_L)$, where S_R and S_L correspond to flux densities in the RC and LC polarized emission for a given detected feature, we have a good estimate of the percentage of circular polarization P. For each polarized feature listed in Table 2 we measured in the other sense of polarization the corresponding flux density to estimate P, and for each determination of P we estimated an uncertainty from

$$\Delta P = 0.5(1 - P^2)(\Delta S_M/S_M) + 0.5(1 + P^2)(\Delta S_m/S_M)$$

where $\Delta S_M = Max(\Delta S_R, \Delta S_L)$, $\Delta S_m = Min(\Delta S_R, \Delta S_L)$ and $S_M = Max(S_R, S_L)$. We conservatively took $\Delta S_M = \Delta S_m = 3\ \sigma$ from our spectra. Limiting ourselves to those features for which P is greater than the uncertainty obtained in the manner above, we obtained the list of features given in Table 6. The sense of polarization, and the derived values of P (and uncertainty) are given in the fourth and last columns of Table 6, respectively. The sense of polarization is noted R or L to indicate that $S_M = Max(S_R, S_L)$ is either right- or left-circularly polarized. In some cases a given feature may lie at the edge of a strong feature with the other sense of polarization, so the sense of polarization, RC or LC, may be different from the polarization quoted in Table 2. For such features the sense of polarization is given in parentheses in Table 6. Among the 116 features in Table 6 about 34% exhibit polarization $> 70\%$; there are several features having $> 90\%$ polarization. Similarly, a high percentage of circularly polarized radiation is often observed in 18 cm OH masers. It is interesting to note that at 6035 MHz, where the signal is stronger than at 6031 MHz, the distribution of RC and LC features in Table 6 favors RC by about 53% (avoiding uncertain senses of polarization). We also note that in strong 6035 MHz sources the ratio of the RC integrated flux density to the LC integrated flux density favors right-circular polarization; this is the case for W3(OH), 19111+1048, and ON1 (Table 3). However, in several sources, including the intense emission from M17, the total integrated flux density in RC and LC polarization are nearly equal.

The basic theoretical treatment of maser radiation needed for the interpretation of the polarization properties is given in Goldreich et al. (1973). Later it was shown that circular polarization is due to overlap of Zeeman components (Deguchi and Watson 1986), rather than the accidental combination of magnetic field and velocity gradients, as proposed by Cook (1966). Detailed calculations for polarized maser radiation (Nedoluha and Watson 1990) show that the overlap of Zeeman components resulting from velocity differences across the masers may lead to high circular polarization of the OH profiles. We interpret below the polarization properties of maser sources (Table 6) in terms of the Zeeman effect and try to identify Zeeman pairs in our data.

Because the Zeeman effect splits the OH lines, several authors have directly interpreted the frequency separation of left and right circularly polarized features in terms of magnetic field intensities (e.g. Zuckerman et al. 1972 for excited OH). This interpretation is based on the assumption that matching RC and LC polarized components arise from the same spatial location. This hypothesis is strongly supported by VLBI observations of W3(OH) which show indeed that several pairs of features with opposite polarization are spatially coincident (see Moran et al. 1978, and Desmurs et al. 1996 for the 5 cm OH line data, Garcia-Barreto et al. 1988 for the ground-state, and Baudry and Diamond 1996 for the $J = 7/2$ state). Assuming that several of the circularly polarized features in Table 6 are caused by the Zeeman effect we tried to match pairs of features with nearby velocities and opposite senses of polarization (avoiding pairs with one feature lying on the edge of the other feature). Spectra

from 14 sources were found to contain matched pairs. We list these in Table 7. The pairs are identified with the line numbers given for both 6035 and 6031 MHz in column 2 of Table 2. (We discarded 18556+0136 from Table 7 because our 1995 data give an unlikely high magnetic field strength of 20 mG and because all polarization properties of this source are not known; we also note that a single LC feature was observed in our 1994 May spectra as well as in the 1994 March spectra of Caswell and Vaile.) Table 7 contains the center velocity of each pair, and the magnetic field strength derived from the velocity separation of each pair:

Δv (km s^{-1})/H(mG) = 0.056 and 0.079 at 6035 and 6031 MHz.

The possible Zeeman patterns of Table 7 were unambiguously identified except in the case of 19120+1103 where we could have selected the line pairs (2,8), (3,9) and (6,13). The latter case would give a field as strong as that of W3(OH). This is not impossible but we prefer the line pairing given in Table 7 because W3(OH) is so exceptional. In W3(OH) the Zeeman interpretation is strengthened by the fact that our -43 km s^{-1} feature gives the same magnetic field in both main lines, and by our field strength measurements similar to those deduced from the interferometric observations of Moran et al (1978) and Desmurs et al. (1996). However, the single dish measurements cannot supersede interferometric observations which are needed to definitely demonstrate that our candidate Zeeman pairs spatially coincide and thus are actually associated. We also know from VLBI observations that a given velocity feature may be excited in slightly different areas thus making the single dish Zeeman interpretation difficult. Nevertheless, our estimates of the magnetic field seem reliable because they are based on features whose sense of polarization is well established and because we obtain consistent results from the 1994 and 1995 observations (where these are available). Moreover, for the four sources in common with the 18 cm OH sample of Reid and Silverstein (1990) we have similar field strength and same field direction. The field strengths in the 14 sources of our Table 7 span the range 3 to 9 mG, and as pointed out by Caswell and Vaile, there is no field greater than about 10 mG. The 10 mG upper limit is perhaps the maximum field strength allowed in OH masing regions. Presumably this simply reflects the fact that our measurements are made in regions of rather uniform density namely n(H_2) $\approx$ 10^7 cm^{-3}. We note that the field can also be much weaker being about or much less than 3 mG in several sources (W 48, S 68, M17, 19111+1048, 19201+1400, etc.) where we observe that the RC and LC profiles coincide to within 0.18 km s^{-1}. Finally, Table 7 shows that in seven sources we have two or more field determinations at a given epoch and no reversal of the field direction is observed.

In 1974 Davies suggested that the magnetic fields observed in OH maser sources are directed in the sense of the general Galactic rotation. This idea was tested by Reid and Silverstein (1990) who identified reliable Zeeman pairs in 17 sources observed in the 18 cm OH line across the Galaxy. They found that 14 of their sources have line-of-sight field directions aligned in the direction of Galactic rotation. To further explore this suggestion we have added to the fourteen 5 cm OH sources in our Table 7 thirty-two other sources (not in common with us) taken from the works of Caswell and Vaile (19 sources from their Table1) and Reid and Silverstein (13 sources). The source sample taken from Caswell and Vaile was restricted to avoid any overlap with the source sample of Reid and Silverstein and to exclude sources with uncertain field determinations or sources where the field direction seems to reverse or to be complex. In all, we have 46 sources distributed over most of the Galaxy. We stress that there is a qualitative difference between the Reid and Silverstein 18 cm OH sample and our 5 cm/18 cm OH sample of 46 sources, since for 32 sources we do not have 5 cm OH interferometric observations to confirm Zeeman pairs. Nevertheless, we believe that our 5 cm OH restricted sample identifies highly plausible Zeeman pairs. Fig. 9 is a plot in the Galactic plane of the locations of the OH masers and of the line-of sight direction and strength of the magnetic field for all 46 sources. The field strength is indicated by the length of the arrows whose origins mark the Galactic positions. In Table 7 we sometimes give various field determinations (different features, and two epochs); since they are all consistent, the intensity plotted in Fig. 9 is taken to be the average of all measurements. In sources with ambiguous kinematical distances both distance determinations are plotted; these cases are shown with dashed arrows.

Excluding the Galactic center, we find that 28 sources lie in the direction of Galactic rotation (clockwise) and 17 are in the counter-direction. This is statistically different from the results of Reid and Silverstein and from those of Caswell and Vaile who analyzed their data in a manner similar to ours. However, all three works agree that the dominant field alignment is consistent with the direction of Galactic rotation as determined from Faraday rotation measurements and ordered large-scale Galactic magnetic field. Reid and Silverstein and Caswell and Vaile have discussed several effects which may contribute to variations in the line-of-sight field direction and that reversals in the direction of the large-scale Galactic magnetic field are observed. Nevertheless, as suggested in previous work, our Fig. 9 tends to confirm the proposal that OH masers are useful probes of the large-scale structure of the Galactic magnetic field and that the fields deduced from OH masers are of Galactic origin. We do not believe, however, that a simple Galactic star formation process which preserves the field direction is occurring in all cases since Fig. 9 shows several contradictory cases. One can find a number of reasons why the field direction may change. In particular: (i) The field is not dominant, and thus the direction of the field changes during the collapse of high mass stars (see Shu et al. 1987), and (ii) Fragmentation may give rise to regions with different magnetic field strengths. Detailed analysis is beyond the scope of this work and we refer to Heiles et al. (1991) for a critical review of the limitations in using maser sources to determine large-scale magnetic fields.

5. Conclusions

Based on our survey of the two $F = 3 - 3$ and $F = 2 - 2$ main line transitions of the $^2\Pi_{3/2}, J = 5/2$ levels of OH in both

Table 7. Identification of possible Zeeman patterns

Source	Line	1995 July			1994 May	
		Associated Line Numbers[4]	Center Velocity (kms^{-1})	Field (mG)	Center Velocity (kms^{-1})	Field (mG)
W3OH	6035	8,18	-43.03	+8.0	-43.04	+6.4
		5,15	-45.16	+8.7	-45.18	+7.3
		3,13	-47.03	+7.1	-47.08	+4.8
	6031	8,18	-43.01	+8.1	-43.02	+7.7
		6,16	-44.27	+3.3		
		5,14	-45.00	+4.7		
18403-0417	6035	1,3	+94.80	+7.5	+94.78	+6.2
18507+0110	6035	2,5	+62.12	-6.2	+62.09	-6.6
18515+0157	6035	1,2	+45.53	+5.2	+45.54	+5.2
19078+0901	6035	2,9	+10.41	-5.0	+10.40	-5.3
		3,10	+11.08	-5.3	+11.08	-5.5
19120+1103	6035	1,8*	+64.46	-3.2		
		2,9*	+65.10	-5.0		
		3,10*	+65.86	-4.8		
19213+1424	6035	3,8	+55.32	+3.9		
19598+3324	6035	1,3	-19.44	-9.1		
		2,4	-18.68	-5.3		
20081+3122	6035	1,5	-00.64	-2.7		
		4,12	+15.45	-4.8	+15.42	-5.7
	6031	1,2	+14.08	-4.2	+14.06	-3.2
20350+4126	6035	2,4	-09.63	-4.3		
	6031	1,2	-10.93	-2.7	-10.95	-3.2
W75N	6035	1,3	+06.90	+7.8		
		2,4	+08.04	+7.5		
W75S(3)	6035	2,4	-02.19	-3.0		
22176+6303	6035	1,2	-08.16	+2.8		
22543+6145	6035	1,4	-09.91	+4.8		
		2,5	-09.30	+4.8		

[4]Line identification numbers as listed in Table 2

* Another feature pairing although less likely is possible (see text)

senses of circular polarization of 165 sources above $\delta = -29°$ we conclude the following:

1. We have discovered 16 new sources of OH in these transitions, 15 in emission and 1 exhibiting both absorption and emission. We assume that OH emission in the main lines is caused by masering; this is suggested by several properties of our source sample, namely time variability, polarized radiation and narrow linewidths.

2. The 6035 MHz line is more intense than the 6031 MHz line, but the latter is also present in many sources, in contrast to current models of OH maser excitation.

3. If the solid angles of emission for OH and $\approx$ 60-100 μm infrared are equal, then there are a sufficient number of IR photons to populate the $^2\Pi_{3/2}, J = 5/2$ levels.

4. Comparing data for emission lines from the $^2\Pi_{3/2}, J = 3/2, J = 5/2$ and $^2\Pi_{1/2}, J = 1/2$ levels show that the ratio of OH integrated line flux densities to IR flux densities (integrated over the same velocity range) decline from a median value of 7 10^{-3} for the $^2\Pi_{3/2}, J = 3/2$ line to 7 10^{-4} for the $^2\Pi_{3/2}, J = 5/2$ line, and to 1.1 10^{-4} for the $^2\Pi_{1/2}, J = 1/2$ line. Thus, maser pumping efficiency decreases for energy levels which are higher above the ground-state.

5. There is definite evidence for variability over a one year time scale in the 6035 MHz line in the source ON1, and over even shorter periods in several sources in common with the 6035 MHz line survey of Caswell and Vaile (1995). At the other extreme, W3(OH) shows no very clear sign of variability over a 20 year period of time. Between these two extreme examples, there are a number of sources which show some variability. The more intense sources may be saturated masers which are less likely to show rapid time variations.

6. We have derived the percentage of circular polarization in detected sources for 116 features and found that about 34 % had $>$ 70% polarization with several features above 90 % polarization.

7. Using the circular polarization information, we have tentatively identified Zeeman patterns and thus estimated total magnetic field strengths. There is a correlation of the field pattern with the direction of galactic rotation in 28 cases, but in the opposite direction in 17 cases. The large scatter in this correlation may reflect the fact that the direction of the magnetic field is not preserved in the star formation process.

Satellite line absorption or emission from the $^2\Pi_{3/2}, J = 5/2$ levels of OH were also searched toward 19 sources. Sensi-

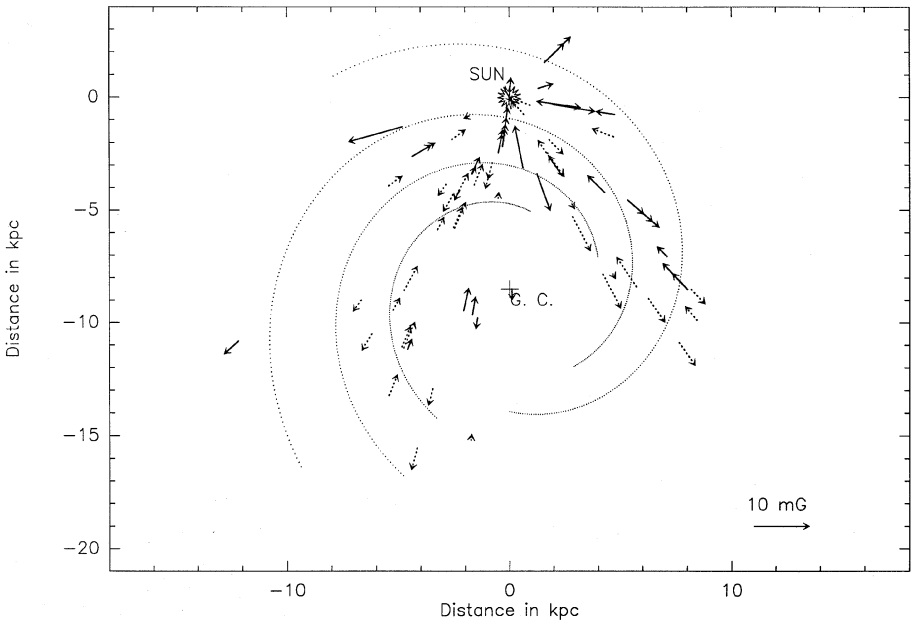

Fig. 9. Plot of 5 and 18 cm OH maser sources on the spiral pattern of the Galaxy. The length and the origin of the arrows indicate the strength of the magnetic field and the position of the OH masers. The 10 mG scale is shown in the bottom right corner. Both distance determinations are plotted in case of ambiguous kinematical distance; these cases are shown with dashed arrows. The spirals are taken from the most recent determination obtained by Y. Georgelin (1995, private communication)

tive measurements of the $F = 3 - 2$ (6049 MHz) and $F = 2 - 3$ (6017 MHz) satellite line transitions have resulted in a detection for the sources W3A and G10.6−0.4, a possible detection in K3−50 and NGC7538, and data for further epochs for W3(OH). In all cases, the $F = 2 - 3$ line is in absorption, the $F = 3 - 2$ line in emission. In W3(OH), there is no hint of time variability and the line intensities are equal in both senses of circular polarization. Thus the 6049 MHz satellite line is not an intense maser. Such behavior is not accounted for in current OH excitation models and will be an important constraint of future models.

Acknowledgements. We thank R. Cesaroni for several useful comments, and we thank both C.M. Walmsley and R. Cesaroni for their help during the observations. We also wish to thank J.L. Caswell for his comments. This work was supported by the CNRS URA No. 352. This research has made use of the SIMBAD database operated at CDS, Strasbourg, France.

References

Andresen P., Ondrey G.S., Titze B., Rothe E.W., 1984, J. Chem. Phys. 80, 2548
Baudry A., Diamond P.J., 1996, A&A in preparation
Baudry A., Menten K.M., 1995, A&A 298, 905
Baudry A., Menten K.M., Walmsley C.M., Wilson T.L., 1993, A&A 271, 552
Brand J., Cesaroni R., Caselli P., et al. 1994, A&AS 103, 541
Bronfman L., Nyman L-A., May J., 1996, A&AS 115, 81
Caswell J.L., Vaile R.A., 1995, MNRAS 273, 328
Cesaroni R., Walmsley M.C., 1991, A&A 241, 537
Codella C., Felli M., Natale V., et al. 1994, A&A 291, 261
Cohen R.J., Baart E.E., Jonas J.L., 1988, MNRAS 231, 205
Cohen R.J., Masheder M.R.W., Caswell J.L., 1995, MNRAS 274, 808
Cohen N.L., Willson R.F., 1981, A&A 96, 230
Cook A.H., 1966, Nature 211, 503
Davies R.D., 1974, IAU Symposium 60, p. 275, eds. Kerr F.J. and Simonson S.C.
Deguchi S., Watson W.D., 1986, ApJ 300, L15
Desmurs J.F. et al., 1996, A&A in preparation
García-Barreto J.A., Burke B.F., Reid M.J.et al., 1988, ApJ 326, 954
Gardner F.F., Martín-Pintado J., 1983-a, A&A 121, 265
Gardner F.F., Martín-Pintado J. 1983-b, MNRAS 204, 709
Goldreich P., Keeley D.A., Kwan J.Y., 1973, ApJ 179, 111
Gray M.D., Doel R.C., Field D., 1991, MNRAS 252, 30
Gray M.D., Field D., Doel R.C., 1992, A&A 262, 555
Guilloteau S., Baudry A., Walmsley C.M. et al., 1984, A&A 131, 45
Guilloteau S., Forveille T., Baudry A et al., 1988, A&A 202, 189
Heiles C., Goodman A.A., McKee C.F., Zweibel E.G., 1991, in Protostars and Planets III, eds. Matthews M. and Levy E.
Kempf A., 1989, unpublished Diploma thesis, Bonn University
Knowles S.H., Caswell J.L., Goss W.M., 1976, MNRAS 175, 537
Kurtz S., Churchwell E., Wood D.S.O., 1994, APJS 91, 659
Moore T.J.T., Cohen R.J., Mountain C.M., 1988, MNRAS 231, 887
Moran J.M., Reid M.J., Lada C.J. et al., 1978, ApJ 224, L67
Nedoluha G.E., Watson W.D., 1990, ApJ 361, 653
Ott M., Witzel A., Quirrenbach A. et al., 1994, A&A 284, 331
Palagi F., Cesaroni R., Comoretto G. et al., 1993, A&AS 101, 153
Pavlakis K.G., Kylafis N.D., 1996, ApJ 467, 300 and 467, 309
Reid M.J., Silverstein E.M., 1990, ApJ 361, 483
Rickard L.J., Zuckerman B., Palmer P., 1975, ApJ 200, 6
Rydbeck O.E.H., Kollberg E., Ellder J., 1970, ApJ 161, L25
Shu F., Adams F.C., Lizano S., 1987, Ann. Rev. A&A 25, 23
Watson W.D., 1993, in "The Structure and Content of molecular Clouds" p. 109, Lectures Notes in Physics No. 439, Springer-Verlag, eds. T.L. Wilson and K.J. Johnston
Wilson T.L., Walmsley C.M., Baudry A., 1990, A&A 231, 159
Yen J.L., Zuckerman B., Palmer P. et al., 1969, ApJ 156, L27
Zuckerman B., Palmer P., Penfield H., et al. 1968, ApJ 153, L69
Zuckerman B., Yen J.L., Gottlieb C.A., Palmer P., 1972, ApJ 177, 59

This article was processed by the author using Springer-Verlag LaTeX A&A style file *L-AA* version 3.